knowledge of its effective heat transport properties is crucial for their optimal design and operation.

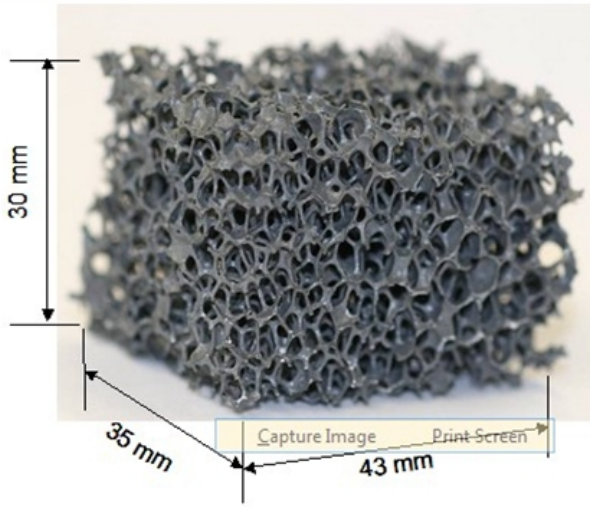

Figure 3.22: Photograph of a Reticulate Porous Ceramic (RPC) made of SiC (average porosity 81%).

The respective information is generated in two steps:

1. Computer tomography (CT), as an experimental technique, is used to obtain the digital geometrical representation of the complex porous structure.

2. The CT-representation is then combined with direct pore-level numerical simulations (DPLS) to accurately determine the morphological and effective heat and mass transfer properties. These include porosity, specific surface area, representative elementary volume, pore size distribution, extinction coefficient, scattering phase function, effective conductivity, heat transfer coefficient, permeability, Dupuit-Forchheimer coefficient, tortuosity, residence time, and dispersion tensor.

The obtained effective properties are intended to be used in a continuum model, developed by spatial average of the governing equation in the fluid and solid phases. This allows for treating the distinct phases as interpenetrating continuum, where the effective properties account for the complex pore-level structure.

3.4.2 Computer tomography

To obtain the exact geometry of complex porous structures CT is used. X-ray radiation has been widely used for radiographic imaging in medical applications and material science. Using the inverse Radon transforms the spatial distribution of X-ray absorption in the material sample can be achieved and therefore the exact 3D geometry can be obtained. A schematic of the principle of CT is shown in Fig. 3.23.

High resolution tomography can e.g. be performed at PSI, Villigen, Switzerland with the TOMCAT beamline of the Swiss Light Source (SLS) The voxel size can range from

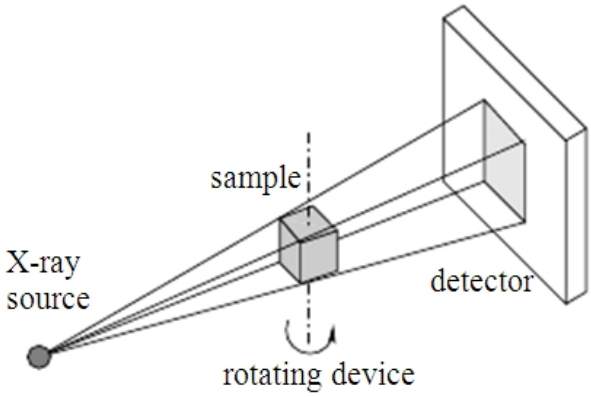

Figure 3.23: Principle of the tomography measurements.

0.09 to 2.8 m, with field of view of 0.18×0.18 to 11.4×11.4 mm^2, respectively. Low resolution can e.g. be performed at EMPA, Dübendorf, Switzerland with higher voxel sizes, from around 10 μm to a few mm. Fig. 3.24 shows an example based on the RPC depicted in Fig. 3.22.

The data obtained by CT consist of 2 byte (0-65535) optical density values, $\alpha(x)$, arranged on a 3D Cartesian grid. The values are segmented to obtain the digital representation of the complex structure. The mode method is used.

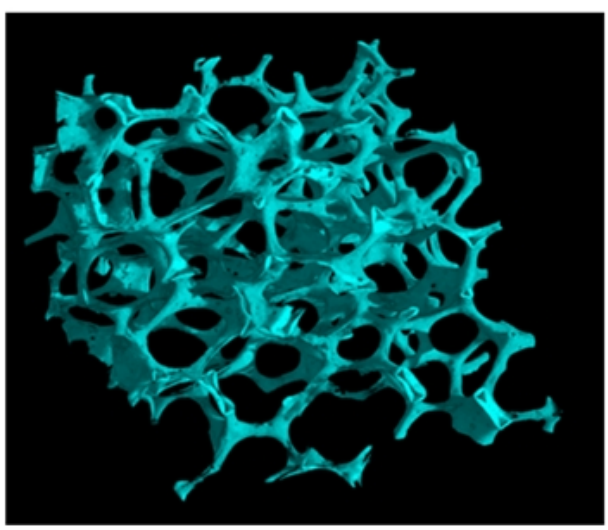

Figure 3.24: 3D digital representation of a RPC sample based on a 25 μm digital resolution X-ray CT scan ("low resolution").

3.4.3 Morphological characterization

Porosity and specific surface area

The two-point correlation function

$$s_2(r) = \frac{\int_V \int_{4\pi} \psi(\mathbf{r})\,\psi(\mathbf{r} + r\hat{\mathbf{s}})\,\mathrm{d}\Omega\,\mathrm{d}V}{4\pi V} \tag{3.8}$$

with its properties $s_2(0) = \varepsilon$ and $\left.\frac{\mathrm{d}s}{\mathrm{d}y}\right|_r = 0 = -\frac{A_0}{4}$ [28] is applied to calculate the porosity and the specific surface area. $s_2(r)$ is computed by Monte Carlo. A random point is chosen within the fluid phase. A second random point is chosen at distance r. If the second point belongs to the fluid phase, the integrand in Eq. 3.8 is equal to 1. Otherwise, it is 0.

Pore size distribution

An opening operation, consisting of erosion followed by dilation with structuring sphere of diameter d, is applied to compute the opening porosity ε_{op} as a function of the diameter d. ε_{op} is then used to determine the RPC's pore size distribution function f [29],

$$F(d) = \int_0^d f(d^*)\mathrm{d}d^* = 1 - \frac{\varepsilon_{\mathrm{op}}(d)}{\varepsilon_0} \tag{3.9}$$

where $\varepsilon_0 = s2(0)$.

Representative elementary volume (REV) size

REV is defined as the minimum volume of a porous material for which the continuum assumption is valid. It is determined based on porosity calculations for subsequent growing volumes until it asymptotically reaches a constant value within a band $\pm\gamma$. The edge length of the cubic REV is defined by [29] :

$$l_{\mathrm{REV},\gamma} = \min\left\{l \le l^* \,\middle|\, \varepsilon - \gamma < \varepsilon(S_{l^*}) < \varepsilon + \gamma\right\}, \quad \gamma < 1 \tag{3.10}$$

where S_{l^*} is a sample sub-volume of edge length l^*.

3.4.4 Heat transfer characterization

Radiative properties

Extinction coefficient, scattering phase function and scattering coefficient are the properties of a participating medium, which describe the radiative behavior. They heavily rely

on the morphology. The complex refractive index of the material is taken for the solid phase [30], which is assumed to be opaque in the visible and near infrared spectral region. The fluid phase is assumed to be radiatively non-participating. Hence, the governing equation of radiative transfer is [31-34] :

$$\frac{\mathrm{d}I_\lambda\left(s,\hat{s}\right)}{\mathrm{d}s}+\beta_\lambda I_\lambda\left(s,\hat{s}\right)=\kappa_\lambda I_{\lambda,b}\left(s,\hat{s}\right)+\frac{\sigma_{s,\lambda}}{4\pi}\int_{4\pi} I_\lambda\left(s,\hat{s}_{\mathrm{in}}\right)\Phi_\lambda\left(\hat{s},\hat{s}_{\mathrm{in}}\right)\mathrm{d}\Omega_{\mathrm{in}} \tag{3.11}$$

where I_λ is spectral radiative intensity; κ_λ, $\sigma_{s,\lambda}$, β_λ are the spectral absorption, scattering, and extinction coefficients; and Φ_λ is the spectral scattering phase function. The spectral subscript λ is omitted in the following text for brevity. Collision-based Monte Carlo method is applied to compute the cumulative distribution functions of the radiation attenuation path s, and the distribution function of the cosine of incidence μ_{in} at the solid wall, $Ge(s)$ and $F_{\mu_{in}}(\mu_{in})$, respectively :

$$G_{\mathrm{e}}\left(s\right)=\int_0^s\frac{1}{N_{\mathrm{r}}}\sum_{j=1}^{N_{\mathrm{r}}}\delta\left(s'-s'_j\right)\mathrm{d}s' \tag{3.12}$$

$$F_{\mu_{\mathrm{in}}}\left(\mu_{\mathrm{in}}\right)=\frac{1}{N_{\mathrm{e}}}\sum_{j=1}^{N_{\mathrm{e}}}\delta\left(\mu_{\mathrm{in}}-\mu_{\mathrm{in},j}\right) \tag{3.13}$$

$Ge(s)$ and $F_{\mu_{in}}(\mu_{in})$ are related to β and Φ by:

$$G_{\mathrm{e}}\left(s\right)\approx 1-\exp\left(-\beta s\right) \tag{3.14}$$

$$\Phi\left(\mu_s\right)=\frac{2\int_{\mu_{\mathrm{in}}=0}^{1}\int_{\varphi_{\mathrm{d}}=0}^{\pi}\int_{\mu_{\mathrm{r}}=0}^{1}\delta\left(\mu_s-\sqrt{\left(1-\mu_{\mathrm{in}}^2\right)\left(1-\mu_{\mathrm{r}}^2\right)}\cos\varphi_{\mathrm{d}}-\mu_{\mathrm{in}}\mu_{\mathrm{r}}\right)\cdot\rho''\left(\mu_{\mathrm{in}},\mu_{\mathrm{r}},\varphi_{\mathrm{d}}\right)F_{\mu_{\mathrm{in}}}\mu_{\mathrm{r}}\mathrm{d}\mu_{\mathrm{r}}\mathrm{d}\varphi_{\mathrm{d}}\mathrm{d}\mu_{\mathrm{in}}}{\int_{\mu_{\mathrm{in}}=0}^{1}\int_{\varphi_{\mathrm{d}}=0}^{\pi}\int_{\mu_{\mathrm{r}}=0}^{1}\rho''\left(\mu_{\mathrm{in}},\mu_{\mathrm{r}},\varphi_{\mathrm{d}}\right)F_{\mu_{\mathrm{in}}}\mu_{\mathrm{r}}\mathrm{d}\mu_{\mathrm{r}}\mathrm{d}\varphi_{\mathrm{d}}\mathrm{d}\mu_{\mathrm{in}}} \tag{3.15}$$

where μ_s and μ_r denote the cosines of scattering and reflection angles. $Ge(s)$ and $F_{\mu_{in}}(\mu_{in})$ are computed by following the histories of a large number of stochastic rays launched at random locations within the fluid phase of the REV. Ne rays interact with the solid-fluid interface by either absorption or reflection. The path length s within REV is recorded for all N_r rays while the cosine of incidence μ_{in} is recorded for all N_e rays [31-34]The intersection point between a ray and the solid-fluid interface is found by following the ray in discrete steps until the normalized gray values are larger than α_t/α_{max}. Finally, the exact determination is achieved by applying the bisection method. Note that the interface is described by a continuous function and no numerical grid is required. E.g. at ETH/PSI the computations can be performed with an in-house Fortran 95 code.

Effective conductivity

The governing steady-state heat conduction equations within the solid and the fluid phases are:

$$0 = \nabla \cdot \left(k_s \nabla T_s \right) \tag{3.16}$$

$$0 = \nabla \cdot \left(k_f \nabla T_f \right) \tag{3.17}$$

The boundary conditions are :

$$T_s = T_f \,,\ \hat{\mathbf{n}} \cdot k_s \nabla T_s = \hat{\mathbf{n}} \cdot k_f \nabla T_f \ \text{at solid} - \text{fluid interface} \tag{3.18}$$

$$\mathbf{q}'' \cdot \hat{\mathbf{n}} = 0 \ \text{at sample lateral walls} \tag{3.19}$$

$$T_s = T_f = T_1 \ \text{at sample inlet} \tag{3.20}$$

$$T_s = T_f = T_2 \ \text{at sample outlet} \tag{3.21}$$

The finite volume (FV) technique with successive over-relaxation is applied to solve the Eqs. 3.163.17. At ETH/PSI the computations are performed with an in-house Fortran 95 code. By applying the 1-equation average model describing the conduction heat transfer in porous media [35, 36], the heat flux can be linked to the effective conductivity by,

$$k_e = l \frac{-\int_{A_s} k_s \nabla T_s \cdot \hat{\mathbf{n}} \, dA_s - \int_{A_f} k_f \nabla T_f \cdot \hat{\mathbf{n}} \, dA_f}{\left(T_1 - T_2\right)\left(A_s + A_f\right)} \tag{3.22}$$

Effective heat transfer coefficient

The heat flux from the solid to the fluid phase is given by:

$$q = h_{sf} A_{sf} \left(T_{\text{interface}} - T_{mf} \right) \tag{3.23}$$

The coupled continuity, momentum, and energy equations are solved within the fluid phase of a square duct containing a sample of the porous material by using a CFD code [38] to obtain the temperature distribution in the fluid phase and the heat fluxes through the solid-fluid interface. The boundary conditions are :

$$\overline{\mathbf{u}} = 0, \quad T = T_{sf} \ \text{at solid} - \text{fluid interface} \tag{3.24}$$

$$\overline{\mathbf{u}} \cdot \hat{\mathbf{n}} = 0, \ \hat{\mathbf{n}} \cdot \nabla \overline{\mathbf{u}} = 0, \ \mathbf{q}'' \cdot \hat{\mathbf{n}} = 0 \ \text{at sample lateral walls} \tag{3.25}$$

$$\overline{\mathbf{u}} \cdot \hat{\mathbf{n}} = -u_0, \ T = T_0 \ \text{at sample inlet} \tag{3.26}$$

$$p = p_{\text{atm}} \ \text{at sample outlet} \tag{3.27}$$

h_{sf} is then determined as a function of Pr and Re by using:

$$h_{sf} = \frac{\int_{A_{sf}} q'' \, dA_{sf}}{A_{sf} \cdot \Delta T_{lm}} \tag{3.28}$$

At ETH/PSI the mesh is generated with an in-house mesh generator for unstructured body-fitted grids. The mesh generator covers the domain by tetrahedral elements and subsequently refines the elements at the phase boundary. Finally, a rounding, cutting and smoothing process is made to achieve an accurate domain representation [38].

3.4.5 Mass transfer characterization

Permeability and Dubuit-Forchheimer coefficient

Darcy's law [40] and its extensions [41, 42] are applied for a fluid flow in an averaged isotropic porous medium,

$$\nabla p = -\frac{\mu}{K}\overline{\mathbf{u}}_{\mathrm{D}} - F_{\mathrm{DF}}\rho\overline{\mathbf{u}}_{\mathrm{D}}\left|\overline{\mathbf{u}}_{\mathrm{D}}\right| \tag{3.29}$$

Non-dimensionalization of Eq.3.29 for the 1-D case yields:

$$\frac{\nabla p \, d^2}{\mu u_{\mathrm{D}}} = \Pi_{\mathrm{pg}} = -\frac{d^2}{K} - F_{\mathrm{DF}} d \, \mathrm{Re} = -c_0 - c_1 \mathrm{Re} \tag{3.30}$$

The continuity and momentum equations are solved within the fluid phase of a square duct containing a sample of the porous material to obtain the velocity and pressure distributions for the following boundary conditions:

$$\overline{\mathbf{u}} = 0 \text{ at solid} - \text{fluid interface} \tag{3.31}$$

$$\overline{\mathbf{u}} \cdot \hat{\mathbf{n}} = 0, \ \hat{\mathbf{n}} \cdot \nabla\overline{\mathbf{u}} = 0 \text{ at sample lateral walls} \tag{3.32}$$

$$\overline{\mathbf{u}} \cdot \hat{\mathbf{n}} = -u_0 \text{ at sample inlet} \tag{3.33}$$

$$p = p_{\mathrm{atm}} \text{ at sample outlet} \tag{3.34}$$

Tortuosity and residence time distribution

Tortuosity is defined as the ratio of the real length of the connected pore channels to the thickness of the porous sample in the main flow direction,

$$\tau = \frac{l_{\mathrm{path}}}{l_{\mathrm{sample}}} \tag{3.35}$$

The residence time required for a particle to flow through the porous sample is defined as :

$$t = \int_{l_{path}} \frac{1}{u} \cdot dl \tag{3.36}$$

Dispersion tensor

The governing equation coupling the convection and diffusion in the fluid phase is [44] :

$$\frac{\partial c}{\partial t} + \nabla \cdot (c\,\overline{\mathbf{u}}) - \nabla \cdot \left(\overline{\overline{\mathbf{D}}} \cdot \nabla c\right) = 0 \tag{3.37}$$

The dispersion tensor $\mathbf{D}$ in an isotropic medium can be decomposed in parallel and transverse components, D_{II} and $D_{\perp}$, respectively. For zero molecular diffusion,

$$D_i = b_0\,\mathbf{Re}^{b_1} \tag{3.38}$$

with b_0 and b_1 constants. The solution of Eq. 3.39 links $\mathbf{D}$ to the standard deviation of the normally distributed concentration c [44] :

$$\sigma_i = \sqrt{2 \cdot D_i \cdot t} \tag{3.39}$$

D_x, D_y and D_z are determined by following streamlines through the porous material, registering their spatial displacement at a specific time instant (e.g. in z-direction: $\Delta z = z(t) - z(t_0)$), and subsequent fitting the registered distribution to a standard Gauss distribution.

Examples for the application of the characterization method based on CT as described in the subchapters 3-5 above can be found in the references (e.g. [29, 37, 46]).

Nomenclature

a	thermal diffusivity, m^2 s^{-1}
b_0, b_1	constants in Eq. 3.38
A	surface, m^2
A_0	specific surface, m^{-1}
c	concentration, kg m^{-3}
c_0, c_1	constants in Eq. 3.30

$\mathbf{D}$	dispersion tensor, $m^2\ s^{-1}$
d	diameter, characteristic length scale, m
E	Young's modulus, Pa
f	distribution function, m^{-1}
F	probability distribution function
F_{DF}	Dupuit-Forchheimer coefficient, m^{-1}
G	cumulative distribution function
h_{sf}	interfacial heat transfer coefficient, $W\ m^{-2}\ K^{-1}$
I	radiative intensity, $W\ m^{-3}\ sr^{-1}$
k	conductivity, $W\ m^{-1}\ K^{-1}$
k_e	effective conductivity, $W\ m^{-1}\ K^{-1}$
K	permeability, m^2
l or L	length, m
$\hat{\mathbf{n}}$	surface normal vector
N_r	number of rays
N_e	number of extincted rays
p	pressure, $N\ m^{-2}$
$\mathbf{q}''$	heat flux vector, $W\ m^{-2}$
q	heat transfer rate, W
$\dot{Q}$	heat transfer rate per unit of length or surface, $W\ m^{-1}$ or $W\ m^{-2}$
r	distance between two points in the sample, m
$\mathbf{r}$	position vector for spatial coordinates in the sample, m
$\mathbf{Re}$	Reynolds number
s	path length, m
$\hat{\mathbf{s}}$	unit vector of path direction
s_2	two-point correlation function
S	sample subvolume, m^3
t	residence time, s
T	temperature, K
$\mathbf{u}$	velocity, $m\ s^{-1}$
u_D	Darcean velocity (supervicial volume averaged velocity), $m\ s^{-1}$
V	sample volume, m^3
z	sample dimension in z-direciton, m

Greek

α	absorption values of tomographic scans, m^{-1}
β	extinction coefficient, m^{-1}
δ	Dirac delta function
γ	half bandwidth for REV determination
ε	porosity
κ	absorption coefficient, m^{-1}
λ	radiation wavelength, m
μ	dynamic viscosity, kg m^{-1} s^{-1}
μ_{in}	cosine of incidence angle
μ_r	cosine of reflection angle
μ_s	cosine of scattering angle
ν	kinematic viscosity, m^2 s^{-1}
ϕ	phase difference, s
φ_d	difference azimutal angle, rad
ρ	density, kg m^{-3}
ρ"	bidirectional reflectivity, sr^{-1}
Π_{pg}	dimensionless pressure gradient
σ_s	scattering coefficient, m^{-1}
τ	tortuosity, or time delay, s
θ	non-dimensionnal time
Φ	scattering phase function
ψ	pore-scale indicator function (1 = void phase; 0 = solid phase)
Ω	solid angle, sr

Subscripts

atm	atmospheric
b	blackbody
f	fluid
in	incident
mf	mean fluid
op	opening
s	solid
sf	solid-fluid boundary
t	threshold
tot	total
0	initial

Abbreviations

CT	computer tomography
DPLS	direct pore-level numerical simulations
ETH	Federal Institute of Technology, Zurich, Switzerland
PSI	Paul Scherrer Institute, Villigen, Switzerland
REV	representative elementary volume
RPC	reticulate porous ceramic

References

[1] Dincer I., Rosen MA., 2002, Thermal Energy Storage systems and applications. John Wilez & Sons, LTD. ISBN 0-471-49573-5

[2] Zalba B., Marin JM., Cabeza LF., Mehling H., 2003. Review on thermal energy storage with phase change: materials, heat transfer analysis and applications. Applied Thermal Engineering, 23, 251-283

[3] Sharma S.D. and Sagara K. 2005 Latent heat storage materials and systems : A review. Int J. of Green Energy, 2, 1Ű56

[4] Mehling H. and Cabeza L.F. 2008. Heat and cold storage with PCM, Springer.

[5] Agyenim F., Hewitta N., Eames Ph., Smyth M., 2010. Review of materials, heat transfer and phase change problem formulation for latent heat thermal energy storage systems (LHTESS), Renewable and Sustainable Energy Reviews, Vol 14, 2.

[6] Fernandez A.I., Martínez M., Segarra M, Martorell I., Cabeza L.F. 2010. Selection of materials with potential in sensible thermal energy storage. Solar Energy Materials and Solar Cells, Vol 94, 10, 1723-1729

[7] Gil A., Medrano M., Martorell I., Lazaro A., Dolado P., Zalba B., Cabeza LF., 2010. State of the art on high temperature energy storage for power generation. Part 1 - Concepts, materials and modelization. Renewable and Sustainable Energy Reviews, 14, 31-55.

[8] Medrano M., Gil A., Martorell I., Potau X., Cabeza LF., 2010. State of the art on high temperature energy storage for power generation. Part 2 - Case studies. Renewable and Sustainable Energy Reviews, 14, 56-72.

[9] Nishikawa, M. and Saruyama, Y., 1995 Thermochim. Acta 267, 75

[10] Zhang Y., Jiang Y., Jiang Y., 1999 A simple method, the T-history method, of determining the heat of fusion, specific heat and thermal conductivity of phase-change materials, Meas. Sci. Technol. 10, 201-205,

[11] Faik A., Guillot S., Lambert J., Véron E., Ory S., Bessada C., Echegut P., Py X., 2012. Thermal storage material from inertized wastes: Evolution of structural and radiative properties with temperature, Solar Energy 86

[12] Dullien, F., 1979, Porous Media Fluid Transport and Pore Structure, Academic Press, New York.

[13] Touloukian Y.S., Powell R.W., Ho C.Y., Nicolaou M.C., 1973. Thermophysical Properties of Matter, vol. 10, Thermal Diffusivity, IFI Plenum, New York-Washington.

[14] Mahanta N. K., Abramson A. R., 2010, The dual-mode heat flow meter technique: A versatile method for characterizing thermal conductivity, International Journal of Heat and Mass Transfer 53, 5581-5586.

[15] Mikić B.B., Thermal contact conductance; theoretical considerations, Int. J. Heat Mass Trans. Vol 17- 2.

[16] Mina S., Blummb J., Lindemann A., 2007. A new laser flash system for measurement of the thermophysical properties. Thermochimica Acta 455, 46-49.

[17] Parker W.J., Jenkins R.J., Butler C.P., Abbott G.L., 1961. J. Appl. Phys. 32, 1679.

[18] Py X., Calvet N., Olives R., Meffre A., Echegut P., Bessada C., Veron E., Ory S., 2011 Recycled Material for Sensible Heat Based Thermal Energy Storage to be Used in Concentrated Solar Thermal Power Plants, Journal of Solar Energy Engineering, ASME, Vol 133.

[19] Gustafsson S. E, The transient plane-source technique: for measurements of thermal conductivity and diffusivity of solid materials, 1991. Rev. Sci. Instrum. 62(3).

[20] Rides M., Morikawa J., Halldahl L., Hay B., Lobo H., Dawson A., Allen C., 2009 Intercomparison of thermal conductivity and thermal diffusivity methods for plastics, Polymer Testing, Vol 28, 5.

[21] dos Santos W.N.,2008 Advances on the hot wire technique, Journal of the European Ceramic Society 28.

[22] Jannot Y. and Meukam P., 2004 Simplified estimation method for thermal effusivity and conductivity determination with a low cost hot strip. Meas. Sci. Technol. 15, 1932-8

[23] Daw J. E., Rempe J. L., Knudson D. L., Condie K. G., Crepeau J. C.,2008 Viability of Pushrod Dilatometry Techniques for High Temperature In-Pile Measurements, INL

[24] Doncieux A., Stagnol D., Huger ., Chotard T., Gault C., Ota T.,Hashimoto S., 2008 J Mater Sci 43(12)

[25] Patapy C., Gault C., Huger M., Chotard T., 2009 Acoustic characterization and microstructure of high zirconia electrofused refractories, Journal of the European Ceramic Society, Volume 29, (16-15)

[26] Meffre A., Calvet N., Py X., Olives R., Faure R., Tessier-Doyens N., Huger M., 2012, High temperature TESM thermomechanical characterization and assessment of their resistance to thermal shock. Innostock, Lleida .

[27] Lu T. J. and Fleck N. A., 1998 The thermal shock resistance of solids, Acta mater. Vol. 46, No.13

[28] Berryman, J., and Blair, S., 1986, "Use of digital image analysis to estimate fluid permeability of porous material: Application of two-point correlation functions", Journal of Applied Physics, 60, pp. 1930-1938.

[29] Petrasch, J., Wyss, P., Stämpfli, R., and Steinfeld, A., 2008, "Tomography-based multiscale analyses of the 3D geometrical morphology of reticulated porous ceramics", Journal of the American Ceramic Society, 91, pp. 2659-2665.

[30] Palik, E.D., 1998, Handbook of Optical Constants of Solids II, Elsevier.

[31] Lipiǹski, W., Petrasch, J., Haussener, S., and Steinfeld A., "Application of the spatial averaging theorem to radiative het transfer in two-phase media", in Proceedings of the Eurotherm83-Computational Thermal Radiation in Participating Media III, 15-17 April, Lisbon, Portugal, 2009.

[32] Haussener, S., Lipiǹski, W., Petrasch, J., Wyss, P., and Steinfeld, A., "Tomographic Characterization of a Semitransparent-Particle Packed Bed and Determination of its Thermal Radiative Properties", Journal of Heat Transfer, 131, 072701, 2009.

[33] Petrasch , J., Wyss, P., and Steinfeld, A., 2007, "Tomography-based Monte Carlo determination of radiative properties of reticulate porous ceramics", Journal of Quantitative Spectroscopy and Radiative Transfer, 105, pp. 180-197.

[34] Tancrez, M., and Taine, J., 2004, "Direct identification of absorption and scattering coefficients and phase function of a porous medium by a Monte Carlo technique", International Journal of Heat and Mass Transfer, 47, pp. 373-383.

[35] Coray, P., Lipiǹski, W., and A. Steinfeld, 2008, "Experimental and numerical determination of thermal radiative properties of ZnO particulate media", Oh, C. and Sherif, S.A, Proceedings of the 2008 ASME Summer Heat Transfer Conference, Jacksonville.

[36] Kaviany, M., 1995, Principles of Heat Transfer in Porous Media, Springer-Verlag, New York, Berlin, Heidelberg.

[37] Petrasch, J., Schrader, B., Wyss, P., and Steinfeld, A., 2008, "Tomography-based determination of the effective thermal conductivity of reticulate porous ceramics", Journal of Heat Transfer, 103, pp. 032602/1-10.

[38] Ansys Inc., 2006. ANSYS-CFX, www.ansys.com.

[39] Buck, R., 2000, "Massenstrom-Instabilitäten bei volumetrischen Receiver-Reaktoren", PhD thesis, Universität Stuttgart, Germany.

[40] Darcy, H., 1856, Les Fontaines Publiques de la ville de Dijon, Dalmont. Paris.

[41] Dupuit, J., 1863, Etudes theoriques et praciques sur le mouvement des eaux, Dunond, Paris.

[42] Forchheimer, P., 1901, "Wasserbewegung durch den Boden", Zeitschrift des Vereins Deutscher Ingeneure, 45, pp. 1782-1788.

[43] Macdonald, I.F., El-Sayed, M.S., Mow, K., and Dullien, F.A.L., 1979, "Flow through Porous Media - the Ergun Equation revisited", Industrial and Engineering Chemistry Fundamentals, 18, pp. 199-208.

[44] Hirsch, C., 2007, Numerical Computation of Internal and External Flows, 2nd ed., Elsevier, Amsterdam.

[45] Salles, J., Thovert, J.-F., Delannay, R., Prevors, L., Auriault, J.-L., and Adler, P.M., 1993, "Taylor dispersion in porous media. Determination of the dispersion tensor", Physics of Fluids, 5, pp. 2348-2376.

[46] Haussener S., Coray P., Lipiǹski W., Wyss P., Steinfeld A., 2010, "Tomography-Based Heat and Mass Transfer Characterization of Reticulate Porous Ceramics for High-Temperature Processing", Journal of Heat Transfer, 132, 023305, pp. 1-9.